

## **Influence of cathodic current density on properties of ceramic coatings on 6063 aluminum alloy by micro-arc oxidation**×

Song Chen<sup>1,\*</sup>, Fang Zhang<sup>2,\*</sup>, Decai Qin<sup>1,2</sup>, Haijun Tao<sup>2</sup>, Yangyang<sup>3</sup>, Yunshan Bai<sup>1</sup>

<sup>1</sup>School of Chemistry & Chemical Engineering, Yancheng Institute of Technology, Yancheng, Jiangsu, 224051, PR China

<sup>2</sup>College of Materials Science and Engineering, Key Laboratory of Materials and Technologies for Energy Conversion, Nanjing University of Aeronautics and Astronautics, Nanjing, 210016, PR China

<sup>3</sup>Special and Key Laboratory of Guizhou Provincial Higher Education for Green Energy-Saving Materials, College of information Engineering, Guizhou Minzu University, Guiyang 550025, P.R. China

\*E-mail: [jsyccs@163.com](mailto:jsyccs@163.com), [zhangfang@nuaa.edu.cn](mailto:zhangfang@nuaa.edu.cn)

Received: 16 July 2015 / Accepted: 24 February 2016 / Published: 1 April 2016

---

The ceramic coatings were prepared by a micro-arc oxidation (MAO) process upon 6063 Aluminum Alloy in the environmentally friendly electrolyte of silicate, and the effect of cathodic current density was studied. The results show that cathodic current density plays an important role to obtain a comprehensive performance for the ceramic coating. With the increase of cathodic current density, the color of the coatings gradually changes from light white to brown under natural light. The thickness and the surface micro-hardness of the coatings increase initially and then decrease, the maximum thickness was nearly 5 times thicker than the ordinary one, which is about 13.6  $\mu\text{m}$ . The friction coefficient and the corrosion resistance of the coatings have the same variation trend with the thickness, the surface micro-hardness increases nearly 8 times, the corrosion resistance is almost 10 times better than that of the substrate in 10 min, and the friction coefficient of the coatings is increases 2 times.

---

**Keywords:** Aluminum alloy, Micro-arc oxidation, Micro-hardness, Corrosion resistance, Wear resistance

### **1. INTRODUCTION**

Aluminum and its alloys have a wide range of applications due to their outstanding properties, such as low density, small specific gravity, high specific strength, good thermal conductivity, easy processing, good weld ability and high recovery efficiency[1]. Whereas, the surface of aluminum and

its alloys often show low strength, corrosion resistance, and wear resistance which are unable to meet the design requirements, especially in acidic or alkaline environment[2, 3]. Therefore, further surface treatments for aluminum and its alloys are necessary to realize their real-world applications.

Micro-arc oxidation (MAO) has been developed in recent years, which is a promising technique for metal surface modification. The micro-arc oxidation of ceramic coatings is a in situ anodic oxidation process, which grows a layer of Al, Mg, Ti and other non-ferrous metal or alloy on the surface of substrate and will provide high hardness, excellent corrosion resistance[4-8]. Previously, many researchers have paid much more attentions to obtain high quality MAO ceramic coatings by optimizing the parameters. But the MAO process is very complex, since it has many factors to affect the performance of ceramic coatings, such as species and pH value of electrolyte, electrical parameters of the experiment and the formation mechanism of ceramic coatings [9-13]. Herein, this paper studied the MAO processes for AA 6063 in environmentally friendly electrolyte system. Furthermore, the influence of current density has been further investigated.

## 2. EXPERIMENTAI PROCEDURES

The substrate material is AA 6063, whose chemical composition[14] is shown in Table 1, and the sample size is about 30 mm × 20 mm × 2 mm in Figure 1.

**Table 1.** Composition of AA 6063 (mass %)

Si	Mg	Fe	Cu	Mn	Cr	Zn	Ti	Al	Other impurities
0.2~0.6	0.45~0.9	≤0.35	≤0.1	≤0.1	≤0.1	≤0.1	≤0.1	allowance	Single≤0.1 sum<0.15



**Figure 1.** AA 6063 by micro-arc oxidation treatment

The samples surface were polished using different metallographic sandpapers (600 #, 800 # and 1200 #). Acetone was used as the degreasing agent, and the samples were cleaned in ultrasonic cleaning instrument for 10 min to remove the surface oil, impurities, and then rinsed with distilled water and dried in the air.

The MAO process was conducted as the order: AA Sample → Cutting → Drilling → Rough grinding → Fine grinding → Cleaning → Cleaning and degreasing → Hanging connection → MAO → Post processing.

After MAO, the samples were rinsed with distilled water for 5 minutes in order to remove the residual electrolyte on the surface.

The MAO process was carried out at 40 °C below, and other parameters are given in Table 2.

**Table 2.** The parameters of MAO process

The items	Parameters
Electrolyte composition	Na <sub>2</sub> SiO <sub>3</sub> 8 g/L; NaOH 2 g/L; EDTA2Na 2 g/L; Na <sub>2</sub> WO <sub>4</sub> 1 g/L
Anodic current density	17 A/dm <sup>2</sup>
Cathodic current density	5~14 A/dm <sup>2</sup>
Pulse frequency	100 Hz
Positive duty ratio	20 %
Negative duty ratio	10 %
The oxidation time	10 min

The Coating Thickness Gauge Mini Test 600 was used to measure the thickness of ceramic coatings. Micro-hardness of six different positions was carried out at a load of 1000 g using a HXS-1000A micro-hardness instrument, and the retention time is 15s. Twenty times measurements were conducted for each sample. The corrosion resistance of the substrate and the ceramic coatings was obtained at different cathodic current densities in the corrosive medium of 3.5 % (mass fraction) NaCl solution, which were analyzed by a three-electrode system connected to a CHI 660B workstation. A platinum electrode and a saturated calomel electrode (SCE) were applied as a counter electrode and reference electrode, respectively. The working electrode contacting with the electrolyte had an available area of 1 cm<sup>2</sup>. The potentiodynamic polarization curves were scanning from 0 V to -0.9 V at a scan rate of 1 mV/s at 25 °C. HT-500 wear test machine inspection was used to test friction and wear resistance at the normal load 330 g, frequency of 15 Hz, using the GGr steel ball of  $\phi$ 4 mm for grinding at a retention time for 5 min. Simultaneously, combining German company BRUKER D8-XRD diffraction ceramic coatings phase compositions were analyzed with CuK $\alpha$  radiation over the range of 2 $\theta$  from 20 ° to 80 °. In addition, the size and morphology of the coatings nanostructures were examined by using scanning electron microscope (SEM) from OXFORD INCAX-SIGHT instrument and the corresponding selected area for energy spectrum analysis (EDS).

### 3. RESULTS AND DISCUSSION

#### 3.1. Thickness measurement

The thicknesses of AA ceramic coatings obtained at different cathodic current densities are shown in figure 2. It can be clearly observed that the thickness firstly increased with the increase of cathodic current density, and then declined, suggesting that the coatings thickness increase in a certain range of cathodic current density. When the cathodic current density at  $3.5 \text{ A/dm}^2$ , micro-arc distributed evenly and shortly. Moreover, the thickness of the ceramic coating is about  $11 \mu\text{m}$ , the reaction was relatively soft with the small gas bubbles, while the cathodic current density increased to  $14 \text{ A/dm}^2$ , the thickness of the coating decreased dramatically. This is due to the cathodic voltage increase with the increase of cathodic current density, and the strength of cathodic electric field and the transfer speed of  $\text{Al}^{3+}$  increased, which improve the utilization rate of  $\text{Al}^{3+}$  in the solution. Therefore, the formation number of oxide is relatively increased in a unit time, promoting the growth rate of ceramic coating. But when the thickness increase to a degree, the cathodic voltage constrained to breakdown the coatings[9, 15]. For another, the reduced numbers of coating holes decreasing the gas plasma precipitated evenly accumulated, and reduced the material convey through hole aperture, resulting in decreasing the coatings thickness[16]. However, with increasing the cathodic current density, the electrolyte temperature increase gradually, which also have a certain cathodic dissolved effect on the coatings. From the results, it can be obtained that the maximum thickness value is  $13.6 \mu\text{m}$  and corresponds to the cathodic current density of  $9.8 \text{ A/dm}^2$ .

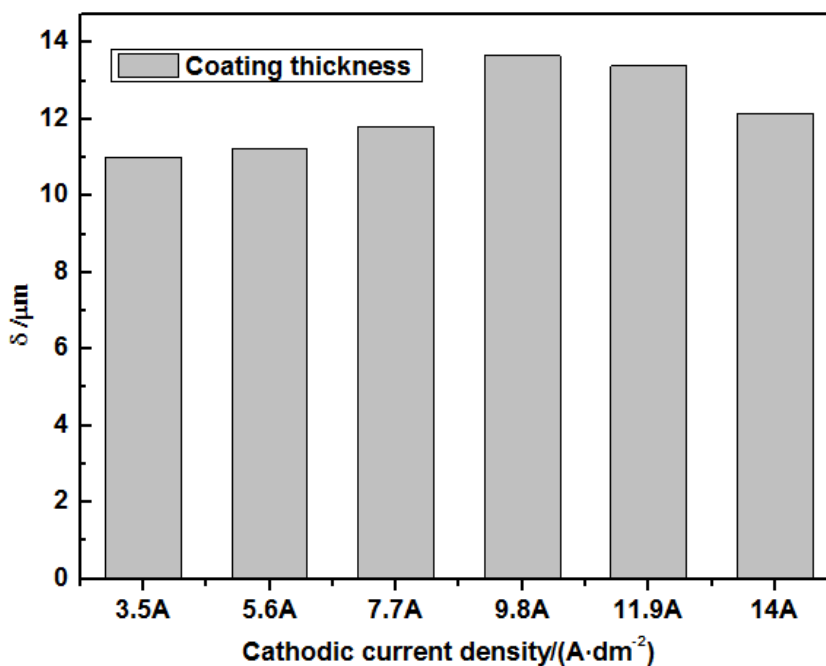


**Figure 2.** the thickness of MAO ceramic coatings obtained at different cathodic current density

## 3.2. SEM observation

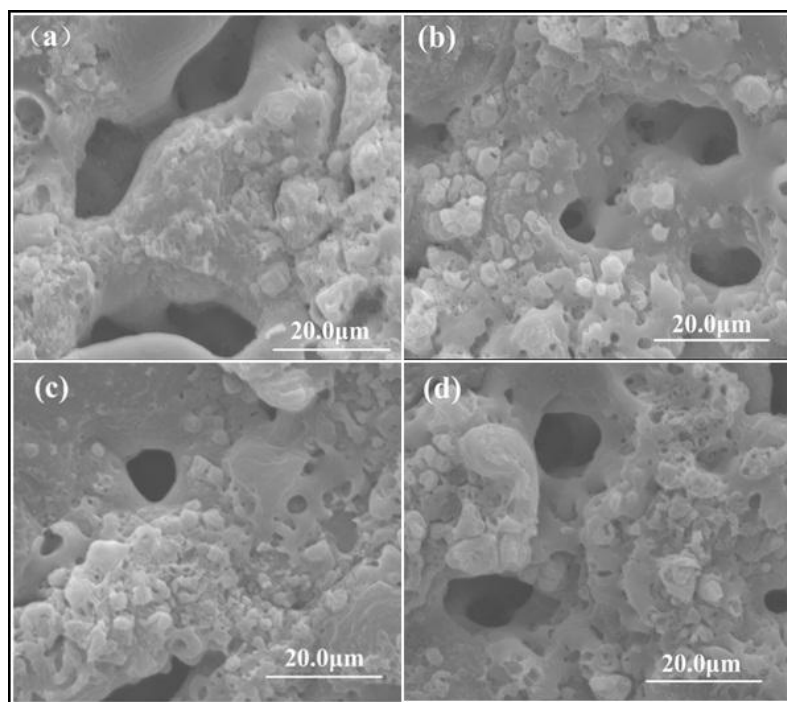


**Figure 3.** SEM micrographs of MAO ceramic coatings fabricated at (a)  $3.5 \text{ A/dm}^2$ , (b)  $7.7 \text{ A/dm}^2$ , (c)  $9.8 \text{ A/dm}^2$ , and (d)  $14 \text{ A/dm}^2$ .

Figure 3 illustrates the effect of different cathodic current densities on microstructure of AA ceramic coatings. It can be seen that, the MAO coating present round cake shaped structure with a center discharge channel. This suggests the melting of the  $\text{Al}_2\text{O}_3$  outflow from the discharge passage, which is formed by the rapid solidification [10, 17, 18]. In addition, it also clearly displayed that the number and diameter of the pores slightly change with increasing the cathodic current density [19] (Figure S1, Supporting Information). With cathodic current density increasing, the number of the micro-pores decreased firstly and then increased slowly. And the pore size has the same variation trend, moreover the roughness degree of the coating keeps the same trend as well. According to the results, the spark generation and its intensity were closely related to the magnitude of cathodic current density [9, 11]. When the cathodic current density was small, the spark density was large, and the formed oxide particles are relatively small as shown in figure 3(a). When increasing the cathodic current density, the spark density decreased, but the spark became larger in volume with stronger discharge energy and higher transient energy [9, 15]. Hence the breakdown occurred, producing more heat in the discharge channel, and the oxide particles produced by discharge after cooling the molten oxide were more obvious in the graph (c), but the coating surface is relatively flatter, and surface roughness accordingly decreased. Because when cathodic current density increased to a certain value, the number of micro-pores increased, the oxide particles became smaller, therefore, the surface roughness decreased [20].

3.3. EDS analysis

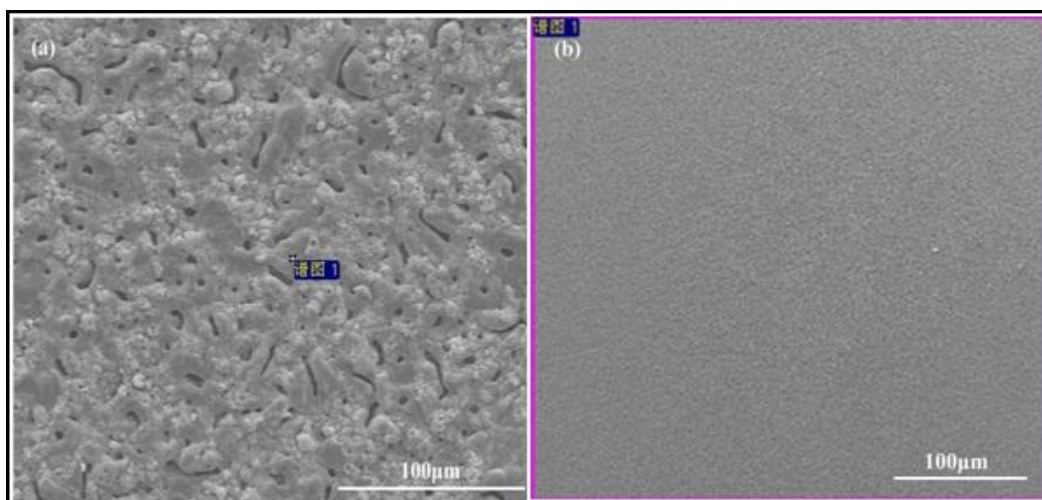


**Figure 4.** EDS scanning mode of MAO ceramic coatings obtained by (a) spot scanning and (b) selected area scanning

Figure 4 shows that there are two EDS scanning mode for ceramic membranes prepared by different cathodic current densities. Figure (a) is for spot scanning and figure (b) for selected area scanning, and each test was repeated for 5 times.

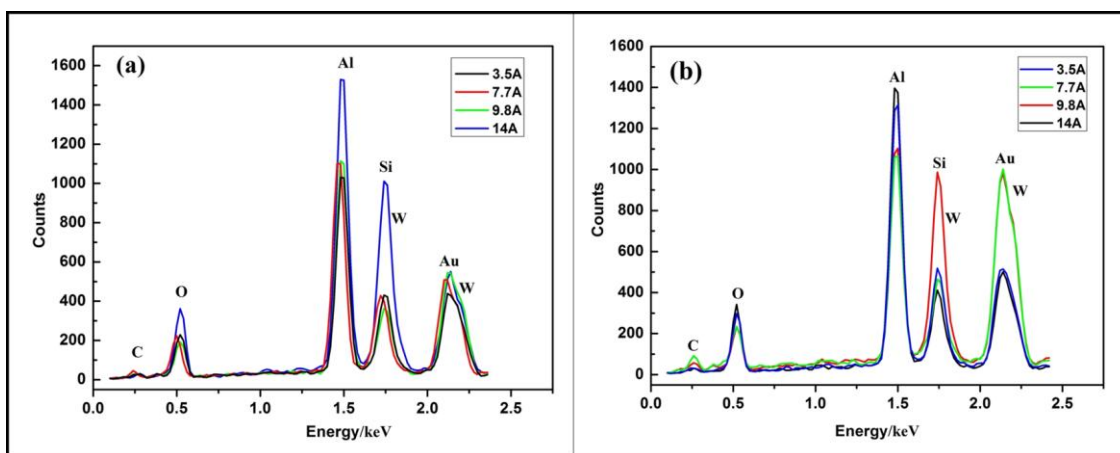


**Figure 5.** EDS spectrum of MAO ceramic coatings obtained by (a) spot scanning and (b) selected area scanning

While Figure 5 is two scanning modes corresponding to each other of EDS (a) and (b) as can be seen, the different scanning modes will not affect the element distribution of the coating, implying better coating quality, and the main components are Al, O, Si and W. In addition, Figure 5 shows that the film element distribution is very uniform with the better quality film. Thus, besides of the most basic oxidation reaction from the substrate Al, the electrolyte ion of  $\text{SiO}_3^{2-}$  was also involved in the reactions [13, 21], from the XRD Atlas of crystal phase behind. The analysis of EDS included W, but

the mass percentage is about 4.6 %, corresponding to the atomic percentage of about 0.50 %, which is less than the content of the third element Si (corresponding percentages are 12.9 % and 9.35 %). In addition, the crystal-phase of  $\text{WO}_3$  has been detected by the XRD diffraction spectrum as well, which only shows a very small peak. Hence, the significantly increased the mutation on W peak at cathodic current density of  $9.8 \text{ A/dm}^2$ , especially selected area scanning mode.

### 3.4. Phase analysis

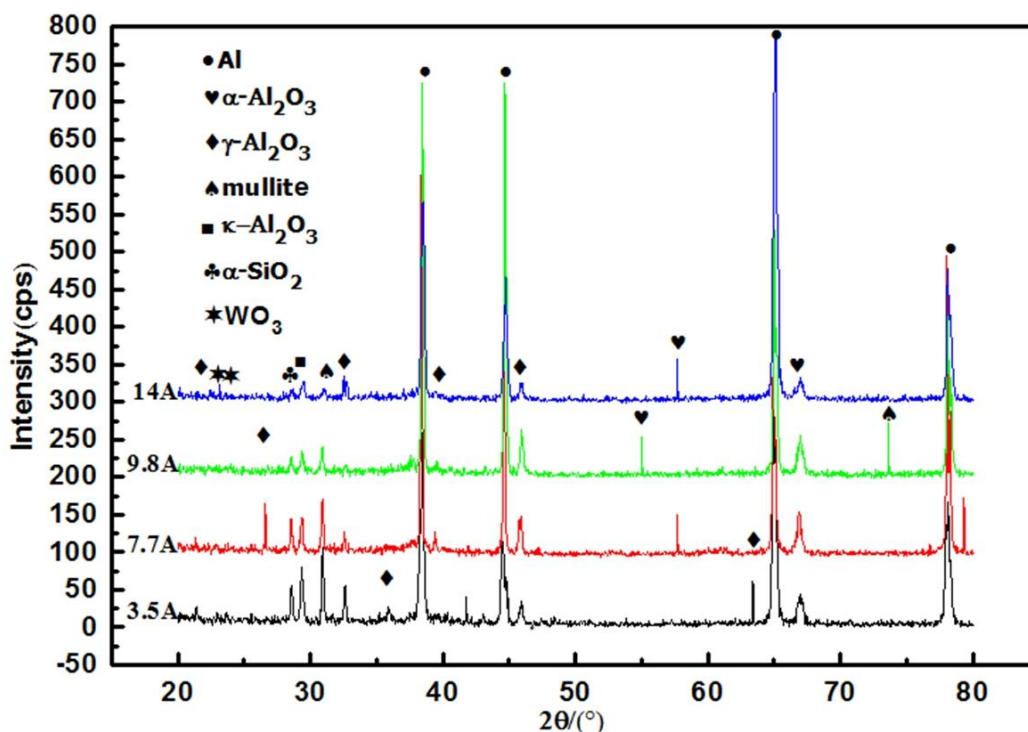


**Figure 6.** XRD patterns of MAO ceramic coatings fabricated at different cathodic current density :  $3.5 \text{ A/dm}^2$ ,  $7.7 \text{ A/dm}^2$ ,  $9.8 \text{ A/dm}^2$ ,  $14 \text{ A/dm}^2$ .

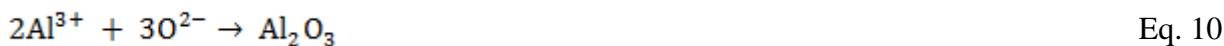
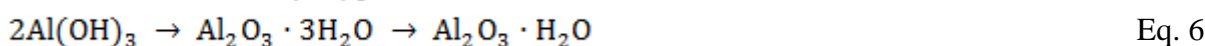
Figure 6 is XRD patterns of the different samples. As can be seen that the coating is mainly composed of Al,  $\alpha\text{-Al}_2\text{O}_3$ ,  $\gamma\text{-Al}_2\text{O}_3$  and mullite[22], which can be learned from the complex reactions of the surface of the AAs during the process of MAO (Eq. 1-11). But the intensity of Al peak is the highest, because X ray penetrates through the coating to the substrate, indirectly showing that the growth of ceramic coating in situ on AA substrates, and also suggesting the thickness is very thin (see figure 2). In addition, for the time of MAO reaction process is only 10 minutes, it is very short. In addition we supply an analysis of the XRD on the MAO reaction time of 30 minutes (Figure S2, Supporting Information), which could verify this phenomenon. Although the plasma discharge in the reaction process, which produced high temperature and pressure on the surface of the substrate. But the reaction time is insufficient, resulting in that a certain content of  $\gamma\text{-Al}_2\text{O}_3$  (Eq. 6) and mullite could not timely change into  $\alpha\text{-Al}_2\text{O}_3$  (Eq. 11).

Moreover, although the temperature was very high at the plasma discharge region, the molten state of alumina will solidified in the electrolyte system (lower temperature), causing the high cooling rate. Thus the main distribution of the external surface layer is  $\gamma$ - $\text{Al}_2\text{O}_3$  phase, which could be directly displayed from the micro-hardness of the coating before and after grinding (figure 7). While the cooling rate near the volcano hole walls will be relatively slow,  $\text{Al}_2\text{O}_3$  phase is easy to form  $\alpha$ - $\text{Al}_2\text{O}_3$  (Eq. 6, Eq. 7)[23]. Besides  $\gamma$ - $\text{Al}_2\text{O}_3$  of external surface layer under high temperature and high pressure environment could be also transformed into  $\alpha$ - $\text{Al}_2\text{O}_3$  (Eq. 11), leading to increase the content of  $\alpha$ - $\text{Al}_2\text{O}_3$ , and further to improve the micro-hardness. Finally, the coating also contains mullite phase,  $\kappa$ - $\text{Al}_2\text{O}_3$  phase (Eq. 7) and  $\alpha$ - $\text{SiO}_2$  phase (Eq. 8, Eq. 9), those phases from complex electrochemical, thermochemical, plasma chemical etc., and processes of MAO[9, 24, 25]. The formation mechanism as follows:

The cathode reaction:



The anodic reaction:



From the above reactions, it can be seen that the MAO is not a simple anode oxidation, but a complex nonfaradaic reaction process[24]. In addition, the pH value of the electrolyte, the electron, water molecules, the electrolyte particles and the electrode metal ions, the reaction process were also accompanied by the material melting, cooling and recrystallization[12, 13, 25, 26].

### 3.5. Ceramic membrane micro-hardness

Figure 7 illustrates the effect of different cathodic current density on micro-hardness of AA ceramic coatings. As previously reported [27, 28], the fabrication of AA coatings by MAO tends to consist of three layers, such as, an outer porous layer, intermediate dense layer and thin inner layer[22]. Herein the micro-hardness of the coating before and after grinding was measured. Because the mechanical property of  $\alpha$ - $\text{Al}_2\text{O}_3$  phase was better than that of  $\gamma$ - $\text{Al}_2\text{O}_3$  phase, the hardness of internal region is higher than outer region[7, 8, 29]. From figure 7, with the increase of cathodic current density, the average micro-hardness of the coatings firstly increased, and then slowly decreased. And the variation tendency of growth rate is in accord with the micro-hardness. When

cathodic current density is  $9.8 \text{ A/dm}^2$ , the micro-hardness reached the maximum, about HV 530.02. And the variation tendency is in accord with the thickness, which indicates that the coating thickness relate to the micro-hardness.

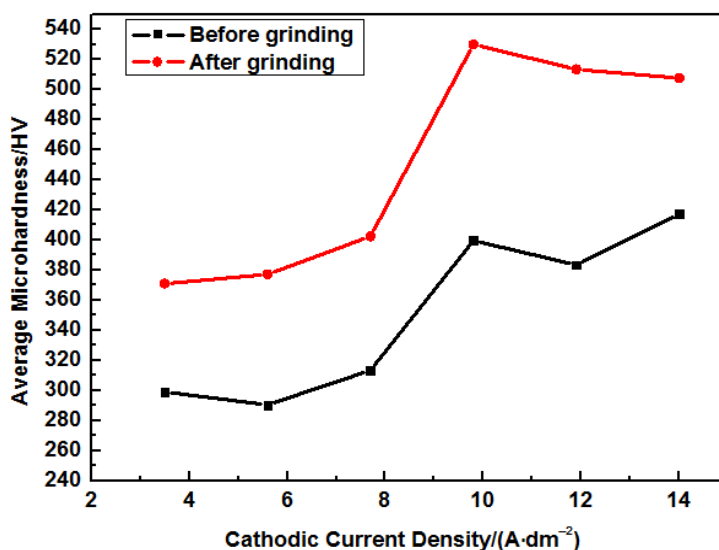


**Figure 7.** Micro-hardness of MAO ceramic membrane obtained at different cathodic current density:  $3.5 \text{ A/dm}^2$ ,  $5.6 \text{ A/dm}^2$ ,  $7.7 \text{ A/dm}^2$ ,  $9.8 \text{ A/dm}^2$ ,  $11.9 \text{ A/dm}^2$ ,  $14 \text{ A/dm}^2$ .

Meanwhile we made a corresponding contrast to the micro-hardness of the cathode and anode current density, which is obviously different, and showed that their mechanism is completely different (Figure S3, Supporting Information). With increasing the ceramic coating thickness, the dense layer thickness increase as well, leading to the content of  $\alpha\text{-Al}_2\text{O}_3$  increase to a certain extent. With the increase of cathodic current density, electrolyte reaction is more intense, micro-arc quantity also gradually increased. From another perspective, the color of the samples observed under the natural light is gradually changes from light white to brown; roughness gradually increased, which is consistent with the literature phenomena[30]. When cathodic current density increased to  $11.9 \text{ A/dm}^2$ , the micro-hardness decreased. Because the cathodic current density is too large, ceramic layer after repeated melting and solidification will eventually destroy the original formation of the evenly coating (Figure S1, Supporting Information), leading to a relatively decline of dense ceramic coating. Therefore, when the cathodic current density increased to  $14 \text{ A/dm}^2$ , a reason of its micro-hardness decreased.

### 3.6. Electrochemical analysis

Figure 8 shows the polarization curves of the samples prepared at different cathodic current densities for measuring the corrosion resistance of AA 6063 ceramic coating, and table 3 lists the relevant polarization parameters. From the above experiments, the coating roughness is more and more obvious under the natural light through naked eye observation. Moreover, the micro-hardness began to

increase and then slow down, indicating that the content of  $\alpha\text{-Al}_2\text{O}_3$  in the coatings firstly increased and then slow down. The thickness, compactness, the number and diameter of the pores and composition phase of the ceramic coating all influence the corrosion resistance [31, 32] From figure 7 and table 3 can be seen, under the constant anodic current density conditions of  $17\text{ A/dm}^2$ , the coatings in different cathodic current density all exhibited an outstanding corrosion resistance than the substrate's. By adjusting cathodic current density, the variation of corrosion potential  $E_{\text{corr}}$  is particularly significant. However, all corrosion potential is much higher than the substrate, suggesting that the corrosion resistance of the coating has been improved[33, 34]. Since the main decisive factor of coating corrosion resistant is dynamical corrosion, the focused on reference is corrosion current  $i_{\text{corr}}$ [35-38].

From table 3, with the increase of cathodic current density, the corrosion current of  $i_{\text{corr}}$  first decreased and then increased. The best corrosion resistance reaches  $7.167 \times 10^{-10}\text{ A}\cdot\text{cm}^2$  at  $9.8\text{ A/dm}^2$  of cathodic current density, and the corresponding corrosion potential is  $-0.374\text{ V}$ , which possesses much higher corrosion potential and lower corrosion current density than the untreated substrate of  $1.080 \times 10^{-8}\text{ A}\cdot\text{cm}^2$  and  $-0.448\text{ V}$ , respectively. The excellent corrosion resistance in this current density is mainly attributed to the thicker film (figure 2), fewer holes and smaller pore size (seen from figure 4c and figure S1c), more  $\alpha\text{-Al}_2\text{O}_3$  phase (figure 6) and good compactness (indirectly reflected in figure 7)[38]. Meanwhile, the high linear polarization resistance  $R_p$ , as well as the high Tafel slope of the cathode and anode made further efforts to explain the performances of the above, which have a lower  $i_{\text{corr}}$  from the Eq. 14 and Eq. 15.

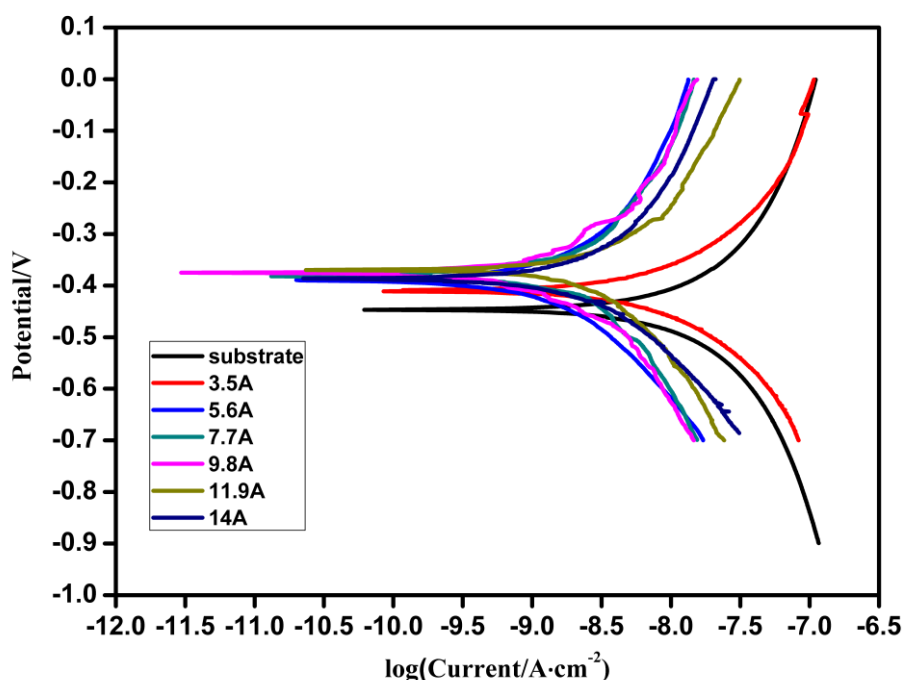


**Figure 7.** Potentiodynamic polarization curves of MAO ceramic coatings obtained at different cathodic current density : substrate,  $3.5\text{ A/dm}^2$ ,  $5.6\text{ A/dm}^2$ ,  $7.7\text{ A/dm}^2$ ,  $9.8\text{ A/dm}^2$ ,  $11.9\text{ A/dm}^2$ , and  $14\text{ A/dm}^2$ .

**Table 3.** Potentiodynamic polarization curves parameters of MAO ceramic membranes obtained at different cathodic current density : substrate, 3.5 A/dm<sup>2</sup>, 5.6A/dm<sup>2</sup>, 7.7A/dm<sup>2</sup>, 9.8 A/dm<sup>2</sup>, 11.9A/dm<sup>2</sup>, and 14 A/dm<sup>2</sup>.

linear polarization resistance

Sample	$i_{corr}/A \cdot cm^2$	$E_{corr}/V$	$R_p(ohm)$
substrate	$1.080 \times 10^{-8}$	-0.448	3983971
3.5A/dm <sup>2</sup>	$6.679 \times 10^{-9}$	-0.411	5702016
5.6A/dm <sup>2</sup>	$1.379 \times 10^{-9}$	-0.389	31858716
7.7A/dm <sup>2</sup>	$2.812 \times 10^{-9}$	-0.383	24907472
9.8A/dm <sup>2</sup>	$7.167 \times 10^{-10}$	-0.374	38489536
11.9A/dm <sup>2</sup>	$3.958 \times 10^{-9}$	-0.370	10957581
14.0A/dm <sup>2</sup>	$2.582 \times 10^{-9}$	-0.401	17263022

3.7. Wear and friction properties

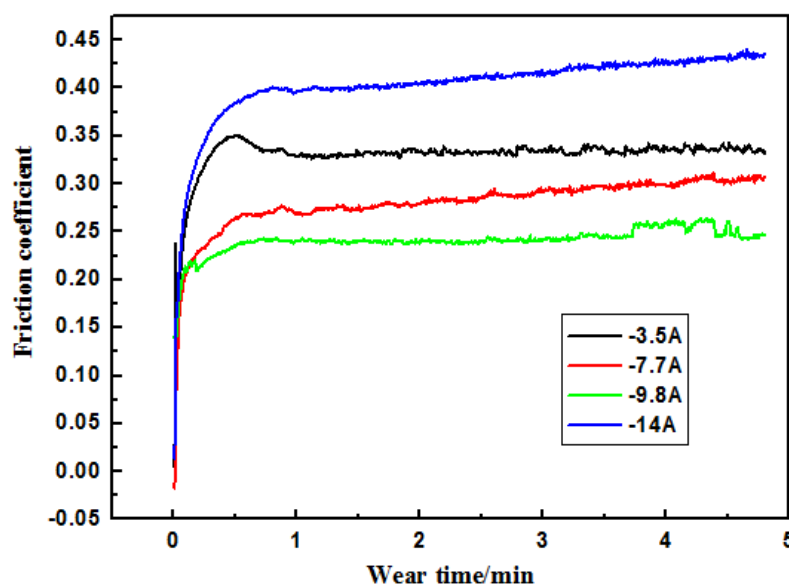


**Figure 9.** Friction coefficient of MAO ceramic coatings fabricated at different cathodic current density: 3.5 A/dm<sup>2</sup>, 7.7A/dm<sup>2</sup>, 9.8 A/dm<sup>2</sup>, (d) 14 A/dm<sup>2</sup>.

Figure 9 illustrates the effect of cathodic current density on wear resistance of AA 6063 ceramic coatings. From figure 9 can be seen, at 9.8 A/dm<sup>2</sup> of cathodic current density shows good friction and wear resistance, the friction coefficient is about 0.237. Friction coefficient curves of ceramic coating formation under different cathodic current density are relatively smooth, indicating that the texture is relatively uniform[5, 28, 41, 42]. However, the size of the various frictions coefficient and different curves tendency could qualitatively analyze the content of  $\alpha$ -Al<sub>2</sub>O<sub>3</sub>, which increases gradually from the surface to the substrate[28, 43]. When cathodic current density is 3.5

A/dm<sup>2</sup>, the friction coefficient is 0.332. The coating roughness under nature light, micro-hardness and thickness after MAO also indicate that the coating has more wear resistance than the substrate of 0.462 (Figure S4, Supporting Information). With cathodic current density increasing, the wear resistance of the coating should increase to a certain extent, the wear resistance is getting better and better[38]. But from figure 9, one abnormal phenomenon of cathodic current density is 14 A/dm<sup>2</sup>, the friction coefficient changed to 0.436, which might be due to large roughness of the coating surface known by their microstructure of AA 6063 ceramic coating and lower  $\alpha$ -Al<sub>2</sub>O<sub>3</sub> phase. At last, it might be due to the thick coating with the loose layer held of the larger proportion of  $\gamma$ -Al<sub>2</sub>O<sub>3</sub> phase from its XRD diffraction patterns.

#### 4. CONCLUSIONS

The effect of different cathodic current densities on the microstructure and property of the coatings have been investigated to further understanding the mechanism of the formation of the coating. It found that when cathodic current density increased gradually, the color of the ceramic coatings gradually changes from light white to brown under natural light. And the thickness and surface micro-hardness of ceramic coating were increase initially and then decrease. In addition, the friction coefficient and corrosion resistance of ceramic coating have the same variation trend. In addition, the optimal value of cathodic current density on the performance of ceramic coating according to the industrial requirement of different productions is determined by experiment. Finally, the AAs' performance by MAO process has been greatly improved, which is far better than those obtained by the other surface treatment technologies. In 10 min, the thickness is 13.6  $\mu$ m, increasing nearly 5 times than that of ordinary anodic coatings. The surface micro-hardness of ceramic coating increased nearly 8 times than the AA 6063 substrate. Simultaneously, the corrosion resistance is better than that of the AA 6063 substrate as well, which increased nearly 700 times. Moreover, the ceramic coatings show excellent wear resistance and the friction coefficient increased by 2 times. The results from the present experiments directly demonstrate the MAO coatings with excellent performance, which fully proves the superiority of this technology. In addition, the electrolyte used in this process is innocuous to the environment and can be used repeatedly. Although the better performance of ceramic coating is obtained by this experiment, the superior performance is possible to obtain by optimizing the other parameters. And this technology is not limited by the shape of the product. Furthermore, we can also produce different colors of ceramic coating as a handicraft. Hence, this technique is completely qualified for the common anodic oxidation process to prepare a comprehensive performance for the ceramic coating in industrial productions.

#### ACKNOWLEDGMENTS

The present work was financially supported by the Institute of materials science and technology from Nanjing University of Aeronautics, the Yancheng City Cooperative Innovation Fund Project (Grant No. YKA201219), the Priority Academic Program Development (PAPD) of Jiangsu Higher Education Institutions, the Natural Science Project of Education Department of Guizhou Province (No. [2015]424) and the Joint Foundation of Science and Technology Department of Guizhou Province (No. [2015]7220).

**References**

1. R. F. Zhang, H. W. Shi, Z. L. Liu, S. F. Zhang, Y. Q. Zhang and S. B. Guo, *Appl. Surf. Sci.*, 289 (2014) 326.
2. Y. Yang and L. Zhou, *J. Mater. Sci. Technol.*, 30 (2014) 1251.
3. H. Chen, J. M. Hao, D. X. Li and L. P. Li, *Appl. Chem. Eng., Pts 1-3*, 236-238 (2011) 1954.
4. Q. M. Zhao, X. Guo, X. Q. Dang, J. M. Hao, J. H. Lai and K. Z. Wang, *Colloid Surf. B*, 102 (2013) 321.
5. W. Yang, A. Y. Wang, P. L. Ke and B. L. Jiang, *Acta Metall. Sinica*, 47 (2011) 1535.
6. Y. M. Wang, J. W. Guo, J. P. Zhuang, Y. B. Jing, Z. K. Shao, S. Jin, J. Zhang, D. Q. Wei and Y. Zhou, *Appl. Surf. Sci.*, 299 (2014) 58.
7. L. T. Duarte, C. Bolfarini, S. R. Biaggio, R. C. Rocha-Filho and P. A. Nascente, *Mater. Sci. Eng.. C, Mater. Biol. Appl.*, 41 (2014) 343.
8. H.-y. Ding, Z.-d. Dai, S. C. Skuiry and D. Hui, *Tribol. Int.*, 43 (2010) 868.
9. W. Yang, B. Jiang, A. Wang and H. Shi, *J. Mater. Sci. Technol.*, 28 (2012) 707.
10. W. Yuan-Hong, O. Jia-Hu, L. Zhan-Guo, W. Ya-Ming and W. Yu-Jin, *Appl. Surf. Sci.*, 307 (2014) 62.
11. X. Wu, Q. Liu and H. Li, *Micro-Nano Technol. Xv*, 609-610 (2014) 14.
12. P. I. Butyagin, Y. V. Khokhryakov and A. I. Mamaev, *Proceedings*, 3 (2004) 101.
13. M. M. S. Al Bosta and K.-J. Ma, *Infrared Phys. Technol.*, 67 (2014) 63.
14. V. Mohanavel, M. Karthick and D. L. B. Paul, *Int. J. Appl. Eng. Res.*, 10 (2015) 12475.
15. B. Zou, G.-h. LÜ, G.-l. Zhang and Y.-y. Tian, *Trans. Nonferrous Met. Soc. China*, 25 (2015) 1500.
16. J.-H. Wang, M.-H. Du, F.-Z. Han and J. Yang, *Appl. Surf. Sci.*, 292 (2014) 658.
17. Y. Xiong, C. Lu, C. Wang and R. G. Song, *Appl. Surf. Sci.*, 322 (2014) 230.
18. S. Dejiu, C. Jingrui, L. Guolong, H. Donglei, W. Lailei, M. Haojie, X. Yonghong, C. He and Y. Yaqian, *Vacuum*, 99 (2014) 143.
19. Y. Yang and H. Wu, *Trans. Nonferrous Met. Soc. China*, 20 (2010) S688.
20. W. Liu, W. Liu and A. Bao, *Procedia Eng.*, 27 (2012) 828.
21. Y.-H. Wang, Z.-G. Liu, J.-H. Ouyang, Y.-M. Wang and Y. Zhou, *J. Alloys Compd.*, 647 (2015) 431.
22. W. C. Gu, D. J. Shen, Y. L. Wang, G. L. Chen, W. R. Feng, G. L. Zhang, S. H. Fan, C. Z. Liu and S. Z. Yang, *Appl. Surf. Sci.*, 252 (2006) 2927.
23. Q. Jin, W. B. Xue, X. J. Li, Q. Z. Zhu and X. L. Wu, *J. Alloys Comp.*, 476 (2009) 356.
24. L. Xinghua, Z. Liqun, L. Huicong and L. Weiping, *Appl. Surf. Sci.*, 293 (2014) 12.
25. M. M. S. Al Bosta and K.-J. Ma, *Appl. Surf. Sci.*, 308 (2014) 121.
26. L. Wen, Y. M. Wang, Y. Jin and D. B. Sun, *J Phys Conf Ser*, 419 (2013).
27. L. Wen, Y. M. Wang, Y. Jin and D. B. Sun, *Rare Metal Mat. Eng.*, 43 (2014) 1582.
28. F. Zhou, Y. Wang, F. Liu, Y. D. Meng and Z. D. Dai, *Wear*, 267 (2009) 1581.
29. A. E. Gulec, Y. Gencer and M. Tarakci, *Surf. Coat. Technol.*, 269 (2015) 100.
30. W. Yan, W. Dongbo, Y. Jie and D. Shichun, *J. Mat. Sci. Technol.*, 30 (2014) 984.
31. W. T. Hou and Z. X. Kang, *Int. J. Electrochem. Sci.*, 8 (2013) 5613.
32. L. R. Krishna and G. Sundararajan, *Jom*, 66 (2014) 1045.
33. Y. H. Gu, X. J. Cai, Y. J. Guo and C. Y. Ning, *Mater. Des.*, 43 (2013) 542.
34. S. Wu, Y. Zhang, Z. L. Wei, Y. Sheng, X. H. Zhou and Q. R. Chen, *Int. J. Electrochem. Sci.*, 9 (2014) 4394.
35. C. Monticelli, A. Balbo, V. Grassi and F. Zucchi, *Metall Ital.*, 9 (2013) 5.
36. Y. Yang and Y. Liu, *J. Mater. Sci. Technol.*, 26 (2010) 1016.
37. J. J. Xi and J. Zhao, *J. Environ. Sci. Technol., Pts 1-6*, 518-523 (2012) 632.
38. C.-J. Hu and P.-H. Chiu, *Int. J. Electrochem. Sci.*, 10 (2015) 4290.
39. Elsener B. *Corros. Sci.* 47 (2005) 3019.

40. Stern M, Geaby A L. *J. Electrochem. Soc.* 104 (1957) 56.
41. P. A. Vityaz', A. I. Komarov, V. I. Komarova and T. A. Kuznetsova, *J Frict Wear+*, 32 (2011) 231.
42. E. Arslan, Y. Totik, E. E. Demirci and I. Efeoglu, *Surf. Coat. Technol.*, 214 (2013) 1.
43. J. M. Lee, S. B. Kang and J. Han, *Wear*, 264 (2008) 75.

SUPPORTING INFORMATION

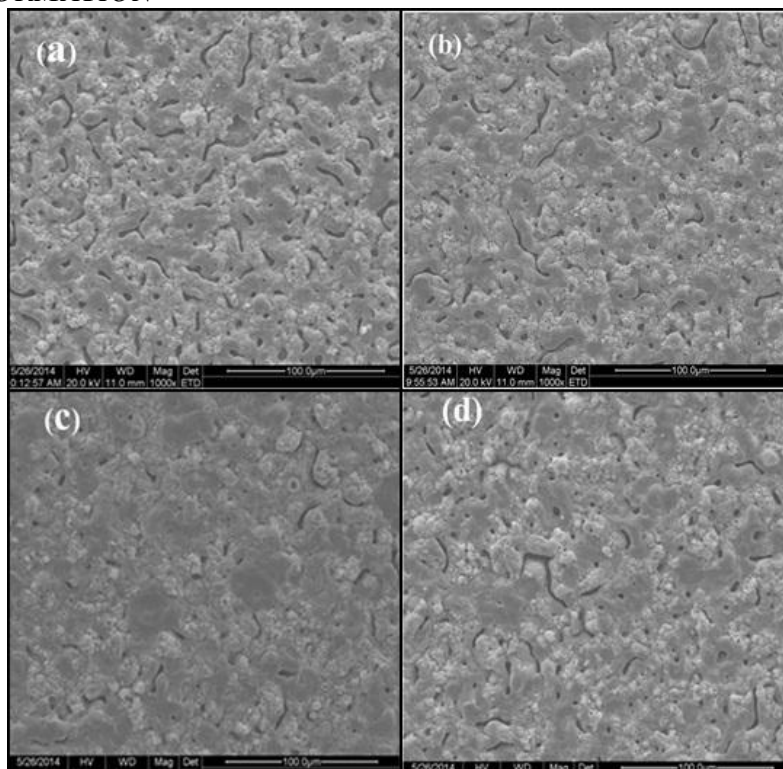


Figure S1. SEM micrographs of MAO ceramic coatings fabricated at (a) 3.5 A/dm<sup>2</sup>, (b) 7.7A/dm<sup>2</sup>, (c) 9.8 A/dm<sup>2</sup>, and(d) 14 A/dm<sup>2</sup>.

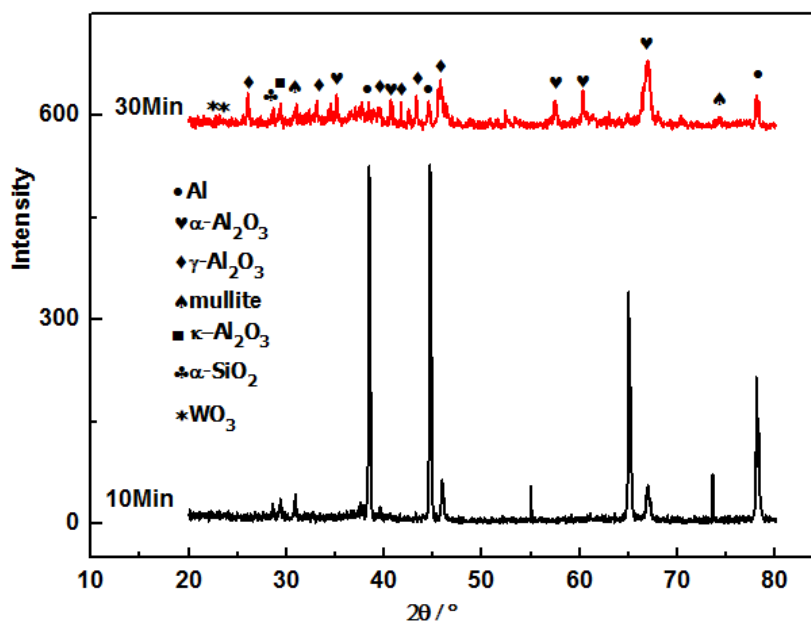
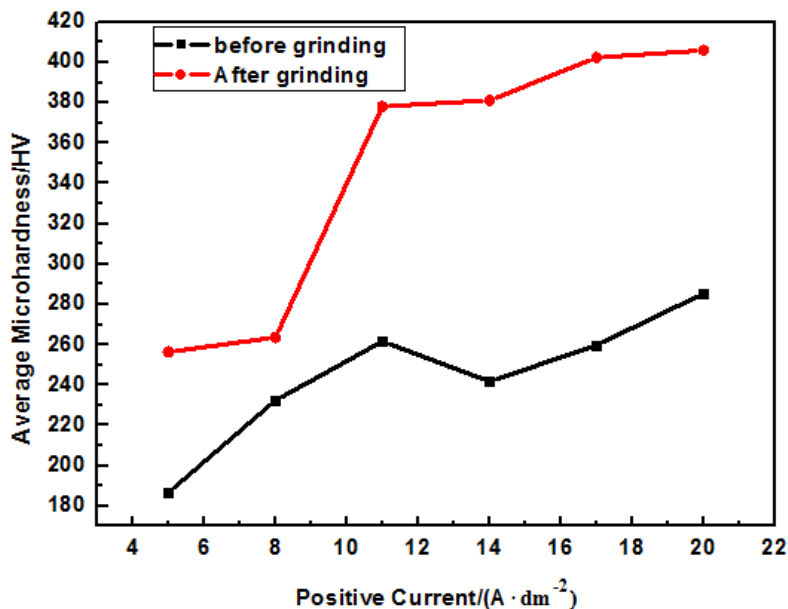
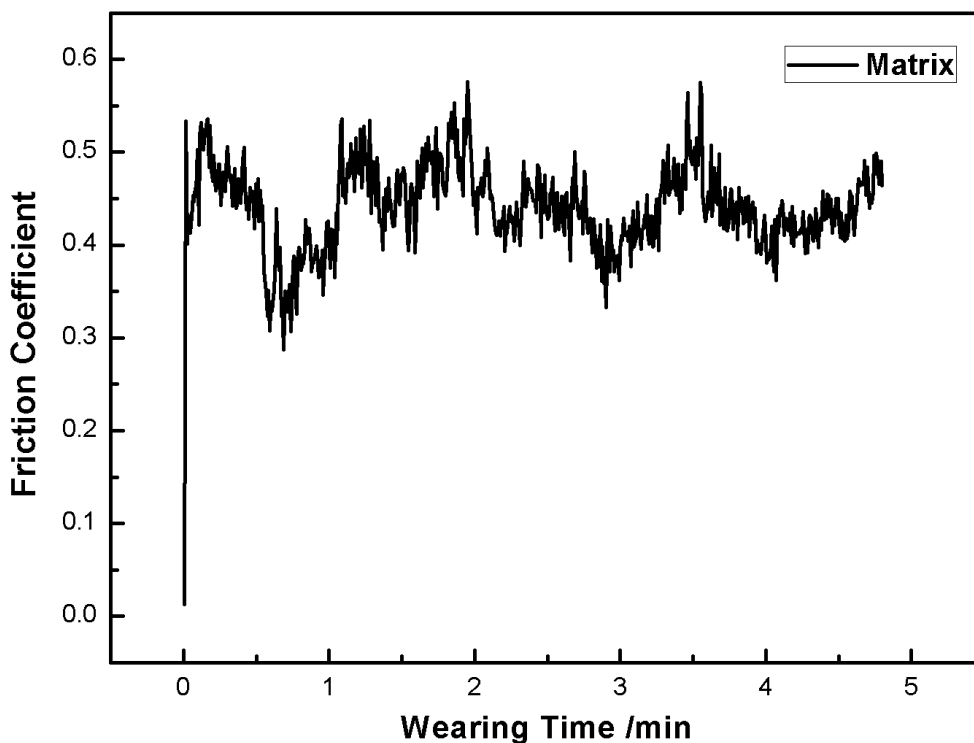


Figure S2. XRD patterns of MAO ceramic coatings fabricated for 30 min



**Figure S3.** Microhardness of MAO ceramic membrane obtained at different positive current density : 5  $A/dm^2$ , 8 $A/dm^2$ , 11 $A/dm^2$ , 14 $A/dm^2$ , 17  $A/dm^2$ , 20 $A/dm^2$



**Figure S4.** Friction coefficient of AA 6063 obtained at substrate